Finite-size effects of hadron masses in lattice QCD: A comparative study for quenched and full QCD simulations

S. Aoki,[1] T. Umemura,[1] M. Fukugita,[2] N. Ishizuka,[1] H. Mino,[3] M. Okawa,[4] and A. Ukawa[1]
[1]*Institute of Physics, University of Tsukuba, Tsukuba, Ibaraki 305, Japan*
[2]*Yukawa Institute, Kyoto University, Kyoto 606, Japan*
[3]*Faculty of Engineering, Yamanashi University, Kofu 404, Japan*
[4]*National Laboratory for High Energy Physics (KEK), Tsukuba, Ibaraki 305, Japan*
(Received 23 December 1993)

A study of finite-size effects is carried out for hadron masses in the quenched simulation of lattice QCD using the Kogut-Susskind quark action. It is found that finite-size effects for quenched QCD are much smaller than those for full QCD, when hadron masses for the two cases are compared at the same physical lattice size and lattice spacing. Based on an extensive study of the boundary condition dependence of hadron masses we ascribe the origin of the difference to a partial cancellation of the finite-size effects among the $Z(3)$-related gauge configurations in quenched QCD; such a cancellation does not take place in full QCD due to $Z(3)$ breaking effects of dynamical quarks. However, this does not mean finite-size errors are negligible in quenched QCD for lattice sizes of 2 to 3 fm used in current simulations; a still significant finite-size shift of hadron masses, especially of the nucleon mass, would pose a serious hindrance to obtaining the hadron mass spectrum at the few percent level aimed at in current quenched QCD simulations.

PACS number(s): 12.38.Gc, 11.15.Ha

I. INTRODUCTION

Understanding finite-lattice-size effects is a basic step towards a quantitative determination of the hadron mass spectrum through numerical simulations of lattice QCD. In a recent simulation in full QCD with dynamical quarks, a substantial lattice size dependence of hadron masses is found for spatial lattice sizes up to about $La \approx 2$ fm [1] (see also [2–4]). It was also observed that the size dependence for small sizes is well described by a power law [5] rather than the exponential expected from analytical considerations for point particles in a finite box [6]. These findings in full QCD raise the question whether a large finite-size effect is also present in hadron masses in quenched QCD, whereas our impression obtained from previous quenched simulations is that it is perhaps not so large [7]. A comparative study of the problem between quenched and full QCD should help us gain insights into possible roles that dynamical sea quarks play in the large finite-size effects in full QCD.

The question of finite-size effects in quenched hadron masses, in fact, has been addressed in a number of previous works. Already in the very early studies on small lattices with limited statistics [8–10] (see also Ref. [11]), the propagation of quarks wrapping around the lattice in the spatial directions was identified as a major source of finite-size effects and methods for eliminating such contributions from hadron propagators were proposed. More recent simulation for Wilson [12–14] and Kogut-Susskind [15,16] quarks actions attempted to quantify the magnitude of finite-size effects without, however, finding conclusive results; for the Wilson quark action, the recent GF11 result [14] reports a sizable decrease of nucleon and ρ meson masses between the lattice size of $La \approx 2$ to 3 fm at $\beta = 6/g^2 = 5.7$ from an analysis combining hadron propagators with a Gaussian sink of size 0, 1, and 2. (For the sink size 4, however, no significant size effect is seen.) Previous studies [12,13] including those by the APE Collaboration [12] at the same value of β and similar lattice sizes did not observe appreciable size effects. For the Kogut-Susskind quark action, lattice-size-dependent masses have occasionally been reported [15,16]. Large statistical fluctuations in hadron propagators for this action, however, do not allow us to conclude whether they represent a real effect. We should note that these studies mostly explored relatively large lattice sizes in the range of 2–3 fm at a rather strong coupling of $\beta = 5.7$ with $a \approx 0.2$ fm, while quenched data for small lattice sizes below 2 fm at a smaller lattice spacing $a \approx 0.1$ fm are needed for a direct comparison with our full QCD data that exhibit a large finite-size effect [1].

In this article we report on a comparative study of finite-size effects for hadron masses in quenched and full QCD with the Kogut-Susskind quark action. For this purpose we have carried out a quenched hadron mass measurement with Kogut-Susskind quarks at $\beta = 6/g^2 = 6.0$ and the quark mass $m_q a = 0.01$, 0.02 on a lattice of a size $L^3 \times 40$ with the spatial lattice size L ranging over $L = 6$–16, supplementing our previous calculation on an $L = 24$ lattice [17]. The physical scale of the lattice spacing estimated from the ρ meson mass is $a = 0.105(3)$ fm, so that the lattice sizes cover $La = 0.6$–2.5 fm. These parameters roughly correspond to those of our full QCD study [1] carried out with two flavors of dynamical Kogut-Susskind quarks at $\beta = 5.7$ on lattices with $L = 8$–20: $a = 0.089(3)$ fm and $La = 0.7$–1.8 fm.

An important parameter for finite-size studies of had-

ron masses is the boundary condition taken for quark fields. One can probe possible effects of hadron sizes relative to that of the lattice through a change of the quark boundary condition in the spatial directions. We have computed hadron propagators employing both periodic and antiperiodic boundary conditions for valence quark fields for some lattice sizes in both quenched and full QCD. In full QCD the boundary condition for dynamical sea quarks is also a parameter. Hence an additional full QCD run on a small lattice of $8^3\times16$ with the quark boundary condition different from that taken in Ref. [1] was also made. The boundary condition for the gluon field is taken to be periodic for all of the simulations. We quote Refs. [9–11] for early studies on the effect of boundary conditions for hadron masses in quenched simulations and Ref. [18] for full QCD.

The ultimate purpose of a finite-size study of hadron masses is to answer the question beyond what lattice size can the size-dependent shift be ignored. This issue will also be discussed briefly.

Finally, another interesting aspect of the finite-size effect is how the chiral U(1) symmetry, which is spontaneously broken for large lattices sizes, becomes restored as the lattice size decreases. The full QCD result at $\beta=5.7$ [1] exhibits a rather abrupt restoration of symmetry at $La\approx1$ fm. The quenched data we have generated for small lattice sizes allow us to make a parallel study for quenched QCD in comparison with full QCD.

This paper is organized as follows. In Sec. II we summarize the parameters and some details of our runs. In Sec. III the results for quenched hadron masses are presented and are compared with those from full QCD. We then present a qualitative argument that allows us to understand the results of the comparison. The argument leads to a variety of testable predictions, and the results are shown. The question of finite-size effects for large lattice size is also discussed. Finite-size effects on the realization of chiral symmetry are examined in Sec. IV. Our conclusions are summarized in Sec. V.

II. DATA SETS

The parameters of lattices employed for our analysis are listed in Table I. For quenched QCD we use $L^3\times40$ lattices with $L=6$, 8, 12, 16, and 24 at $\beta=6.0$. Gauge configurations are generated with the pseudo heat bath algorithm with five hits per link, and hadron propagators are calculated for the quark masses $m_qa=0.01$ and 0.02 in lattice units for every 1000 sweeps with the initial 1000 (10 000) sweeps discarded for $L=6,8$ (12,16,24). The number of configurations used for hadron mass measurements is increased roughly inversely proportionally to the spatial volume L^3 in order to keep statistical accuracy of hadron masses to a similar level for all L. The data for $L=24$ have already been published [17].

The physical value of lattice spacing is estimated from the local ρ meson mass in the $\rho_{VT}(\gamma_k\otimes\xi_k)$ channel (VT denotes vector-tensor) obtained on a $24^3\times40$ lattice extrapolated linearly to $m_q=0$ [17]. The result $a=0.105(3)$ fm and the corresponding physical lattice sizes are also listed in Table I.

TABLE I. Run parameters for hadron mass measurements. Lattice spacing is determined from the ρ meson mass linearly extrapolated to $m_q=0$. b.c. stands for the spatial boundary conditon for the valence quark with P for periodic and AP for antiperiodic. For full QCD data subscripts on the lattice sizes L denote the spatial boundary condition for dynamical sea quarks. Results of full QCD runs are those of Ref. [1] except for the run for $L=8_{AP}$. Quenched configurations are separated by 1000 pseudo-heat bath sweeps, and full QCD runs by five trajectories of unit length with the hybrid R algorithm.

	Quenched runs	Full QCD runs ($N_f=2$)[a]
β	6.0	5.7
$1/a$ (GeV)	1.88(6)	2.23(9)
a (fm)	0.105(3)	0.089(3)
m_qa	0.01, 0.02	0.01, 0.02
L (No. of conf.; b.c.)	6 (800;P,AP)	8_P (160; P,AP)
		8_{AP} (160;P,AP)
	8 (600;P)	12_P (140;P)
	12 (100;P)	
	16 (60;P)	20_P (150–160;P)
	24 (50;P)[b]	
La (fm)	0.63–2.52	0.71–1.78

[a]Reference [1].
[b]Reference [17].

For full QCD we use the data of Ref. [1] for two flavors of dynamical quarks at $\beta=5.7$ and the dynamical quark masses $m_q=0.01$ and 0.02, which were obtained on $8^3\times16$, 12^4, and 20^4 lattices doubled or tripled in the temporal direction for hadron mass measurements, supplementing them with the results on a $16^3\times32$ lattice from Ref. [3]. The physical lattice spacing estimated from the data on a $20^3\times(20\times2)$ lattice in the same manner as for the quenched case above is $a=0.089(3)$ fm. The number of gauge configurations used for hadron mass measurements is 150–160 separated by five trajectories of the hybrid R algorithm for our runs on $8^3\times16$, 12^4, and 20^4 lattices. Increases of statistical fluctuations in hadron propagators toward smaller lattice sizes were relatively mild so that the above number of configurations yielded hadron masses with an accuracy sufficient for our finite-size analysis. This contrasts with the case of quenched QCD, where increasingly larger fluctuations for smaller spatial lattice sizes necessitate larger statistics for hadron mass measurements.

We denote by P the periodic boundary condition in all four directions and by AP the one which is antiperiodic in space and periodic in time. For the gluon field the P boundary condition is employed for all runs. Hadron propagators with the P boundary condition for valence quarks are calculated for all configurations listed in Table I. In addition, the AP boundary condition on valence quarks is used for a $6^3\times40$ lattice for the quenched case and on an $8^3\times(16\times2)$ lattice for full QCD.

In the previous work for full QCD [1,3] the P boundary condition was imposed on dynamical sea quarks. For the present analysis we have made an additional run of 1000 trajectories on an $8^3\times16$ lattice with the AP boundary condition at $m_qa=0.01$. Hadron mass measure-

ments are made for both P and AP boundary conditions for valence quarks on the new configurations periodically duplicated in the time direction.

For the Kogut-Susskind quark action one can construct a large number of hadron operators with a variety of spin-flavor quantum numbers. In the present study we concentrate on the masses of $\pi \equiv \pi(\gamma_5 \otimes \xi_5)$, $\rho \equiv \rho_{VT}(\gamma_k \otimes \xi_k)$, and the local nucleon (N) states.

Valence quark propagators are calculated by the conjugate gradient method with a wall source at $t=0$. For quenched QCD eight wall sources, each with a unit source at one of the corners of every spatial cube, are used to maximize the signal for each channel of hadrons [17]. Simpler wall sources with a unit source at every spatial site or at sites with even coordinate are used for full QCD. To extract hadron masses we fit hadron propagators in a standard manner; with a single exponential for the pion in the Nambu-Goldstone channel or with a sum of two exponentials with an appropriate sign factor $(-1)^t$ for other hadrons, and also adding terms arising from the periodicity in the time direction. The fitting range is chosen to be $t \geq 6$–7 for π, ρ, and N for the quenched case ($t \geq 8$ for π and $t \geq 6$ for ρ and N for full QCD). Errors of masses are estimated by the jackknife procedure. We take each configuration (two successive configurations for $L=6$ and 8) as independent for quenched QCD and ten configurations (i.e., 50 trajectories) as a block for full QCD.

III. FINITE-SIZE EFFECTS OF HADRON MASSES

A. Comparison of quenched and full QCD results

Our chief finding is shown in Fig. 1, where we compare the π, ρ, and N masses obtained for the P boundary condition as a function of the spatial lattice size L for quenched (filled symbols) and full (open symbols) QCD. The conversion to physical units is made with the lattice spacing determined from the ρ meson mass (see Table I). The numerical values of masses in lattice units are summarized in Table II(a) for quenched QCD. The full QCD results from Refs. [1,3] are also recapitulated in Table II(b). The statistical quality of our propagator data is illustrated in Fig. 2, where the nucleon effective mass is plotted for full [Fig. 2(a)] and quenched [Fig. 2(b)] QCD for various lattice sizes.

It is evident in Fig. 1 that the magnitude of finite-size effects toward smaller lattice sizes is much smaller for quenched QCD than for full QCD. The increment of hadron masses due to a finite size for the quenched case is generally a third to a quarter of that for full QCD. Furthermore, the size dependence is more modest; the quenched mass data below $La \approx 2$ fm assuming the form $\Delta_L m \sim L^{-\alpha}$ yield $\alpha \approx 1$–2, which is compared with the value $\alpha \approx 2$–3 observed for full QCD [5].

B. Interpretation of results

Let us try to understand the origin of the difference between quenched and full QCD observed in Fig. 1. We consider a meson propagator $G_M(n) = \langle M_n M_0 \rangle$ on an $L^3 \times \infty$ lattice in an expansion in inverse powers of the valence quark mass $1/m_{\rm val}$. The expansion yields a representation of $G_M(n)$ in terms of closed loops C of valence quarks going through the meson source and sink. The loop C may wind around the lattice in the spatial directions, in which case the corresponding amplitude includes a sign factor $\sigma_{\rm val}$ where $\sigma_{\rm val} = +1$ or $(-1)^n$ for the P or AP boundary condition with n the number of windings around the lattice.

Let us call a loop either Polyakov type or Wilson type depending on whether it winds around the lattice in the spatial directions or not, and denote the corresponding link factor $\mathrm{tr}(\Pi_{l \in C} U_l)$ as $P(C)$ or $W(C)$. The meson propagator can be written as

$$-G_M(n) = \sum_C m_{\rm val}^{-l(C)} \langle W(C) \rangle + \sum_C m_{\rm val}^{-l(C)} \sigma_{\rm val} \langle P(C) \rangle \ , \tag{1}$$

where $l(C)$ is the length of the loop and $\langle\ \rangle$ the gluon field average (including the quark determinant in full QCD).

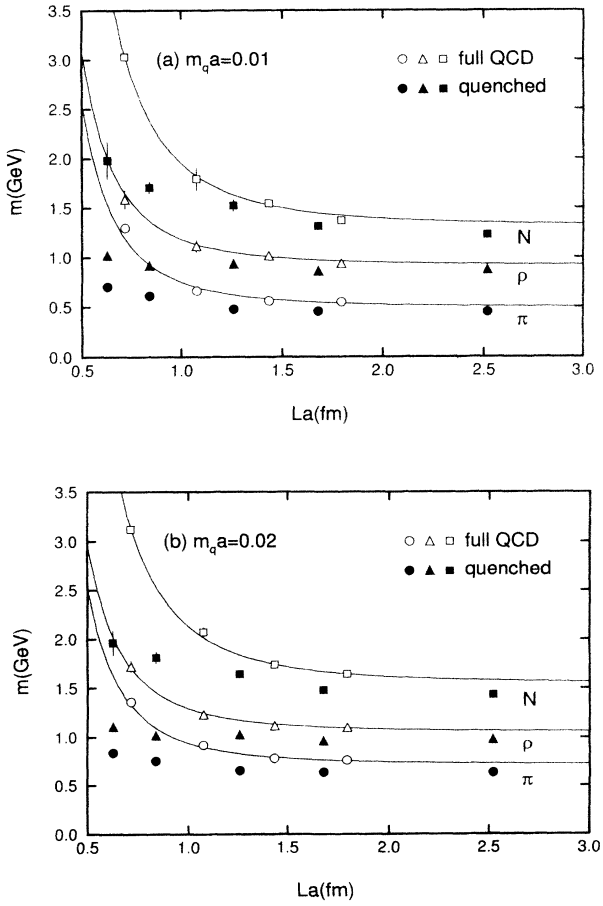

FIG. 1. Comparison of finite-size effects for hadron masses in full (open symbols) and quenched (filled symbols) QCD. Full QCD data at $La \approx 1.4$ fm ($L=16$) are from Ref. [3]. Solid lines are fits of the form $m = m_\infty + c/L^3$ to full QCD data. (a) $m_q a = 0.01$, (b) $m_q a = 0.02$.

TABLE II. Masses of π, ρ, and N for various lattice sizes L. (a) quenched QCD at $\beta=6.0$. Fitting range is $t \geq 6$ for all channels for the size $L \leq 16$ and $t \geq 7$ for $L=24$. (b) full QCD with two flavors of dynamical quarks at $\beta=5.7$. Fitting range is $t \geq 8$ for π and $t \geq 6$ for ρ and N. Periodic boundary conditions are taken for sea and valence quarks.

(a) Quenched QCD

$m_q a$	L	No. of conf.	$m_\pi a$	$m_\rho a$	$m_N a$
0.01	6	800	0.375(11)	0.542(18)	1.053(98)
	8	600	0.3248(55)	0.486(13)	0.907(31)
	12	100	0.2528(29)	0.496(14)	0.812(32)
	16	60	0.2420(16)	0.457(10)	0.699(15)
	24	50	0.2388(10)	0.4654(59)	0.6537(59)
0.02	6	800	0.4430(79)	0.588(10)	1.044(66)
	8	600	0.4004(55)	0.540(11)	0.964(32)
	12	100	0.3474(22)	0.5464(83)	0.859(19)
	16	60	0.3380(13)	0.5116(55)	0.789(10)
	24	50	0.3348(8)	0.5204(32)	0.7615(45)

(b) Full QCD ($N_f=2$)

$m_q a$	L	$m_\pi a$	$m_\rho a$	$m_N a$
0.01	8	0.581(22)	0.711(42)	1.358(4)
	12	0.2963(95)	0.500(29)	0.804(52)
	16[a]	0.252(3)	0.454(4)	0.692(6)
	20	0.2451(23)	0.4184(70)	0.614(11)
0.02	8	0.609(17)	0.772(25)	1.400(13)
	12	0.412(10)	0.552(16)	0.929(21)
	16[a]	0.349(2)	0.501(7)	0.781(10)
	20	0.3403(17)	0.4916(30)	0.7359(53)

[a]Reference [3].

The representation above allows us to distinguish two sources of finite-size effects, one arising from the contribution of Polyakov-type valence quark loops, and the other due to size-dependent changes of gluon field fluctuations that affect the gluon field average. The difference in finite-size effects between full and quenched QCD predominantly originates from the former effect, as we shall discuss below.

The effect of Polyakov-type loops depends on the sign and magnitude of the loop average $\langle P(C) \rangle$ as well as on the value of the sign factor $\sigma_{\rm val}$. It is important to realize that the sign of $\langle P(C) \rangle$ depends on the boundary condition for dynamical sea quarks in full QCD. This is easily seen by constructing an effective potential for the Polyakov loop $P(C)$ for a straight path which winds around the lattice once in some fixed spatial direction, e.g., the x direction. To the leading order in an expansion in inverse powers of the sea quark mass $1/m_{\rm sea}$, the effective potential takes the form

$$S_{\rm eff}(P)=S_0(P)+\sigma_{\rm sea}\, m_{\rm sea}^{-L} \sum_C [P(c)+P(C)^\dagger] , \qquad (2)$$

where S_0 arises from the gluon action and Wilson-type sea quark loops, while the second term is due to sea quark loops winding once around the lattice. The sign factor $\sigma_{\rm sea}=+1$ or -1 for the P and AP boundary condition for the sea quark.

The action $S_0(P)$ is invariant under the center $Z(3)$ symmetry. Hence this term does not distinguish among the three $Z(3)$ directions 1, $e^{2\pi i/3}$, and $e^{4\pi i/3}$ in the complex plane for the Polyakov loop. The second term, on the other hand, breaks the $Z(3)$ symmetry. For the AP boundary condition with $\sigma_{\rm sea}=-1$, this term is more negative toward the positive real axis, while for the P boundary condition ($\sigma_{\rm sea}=+1$) the opposite direction of negative real axis is favored. We then expect that the distribution of Polyakov loops will be shifted toward the positive real axis for the AP boundary condition, resulting in a positive value for the average $\langle P(C) \rangle$. For the P boundary condition, the distribution will be weighted toward the $Z(3)$ directions $e^{2\pi i/3}$ and $e^{4\pi i/3}$, and $\langle P(C) \rangle$ will take a negative value on the average [18]. That these expectations are actually realized is shown in Fig. 3, where we plot the distribution of spatial Polyakov loops for full QCD obtained on an $8^3 \times 16$ lattice for the AP [Fig. 3(a)] and P [Fig. 3(b)] boundary conditions taken for the sea quark.

The discussion above shows that the contribution of Polyakov-type loops to the meson propagator (1) in full QCD is negative for the boundary conditions ($P_{\rm sea}$,$P_{\rm val}$) and ($AP_{\rm sea}$,$AP_{\rm val}$), and positive for ($P_{\rm sea}$,$AP_{\rm val}$) and ($AP_{\rm sea}$,$P_{\rm val}$). Since average values of Wilson-type loops are positive, the two contributions cancel against each

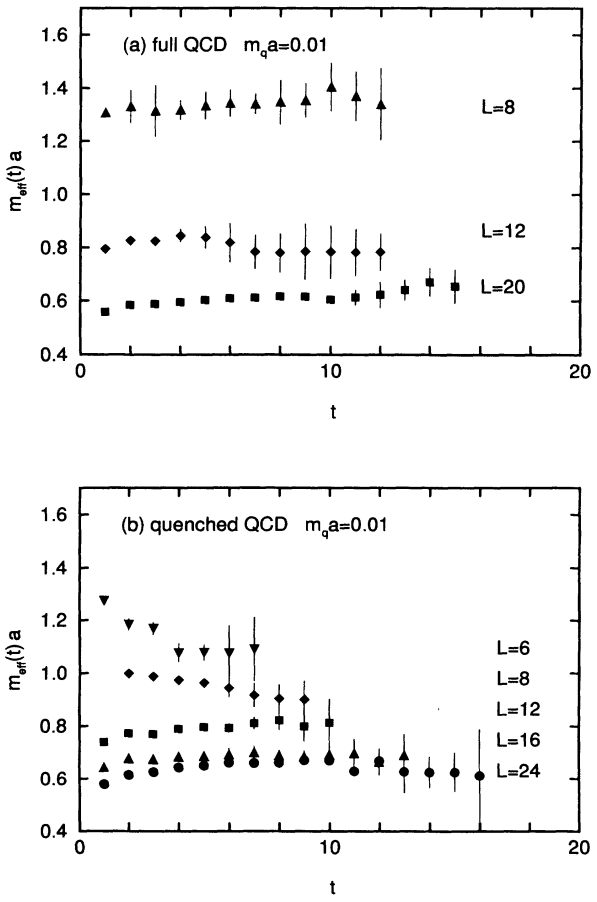

FIG. 2. Nucleon effective masses in lattice units at $m_q a=0.01$ for various lattice sizes for (a) full QCD and (b) quenched QCD.

other for the former two cases. This leads to a faster decrease of the meson propagator, and hence to an increase of meson masses for the cases of (P_{sea}, P_{val}) and (AP_{sea}, AP_{val}) boundary conditions. On the other hand, we expect a decrease of meson masses for the (P_{sea}, AP_{val}) and (AP_{sea}, P_{val}) cases, since the Polyakov-type contributions add up to those of the Wilson-type loops.

For the (P_{sea}, P_{val}) boundary condition an increase of meson masses was already observed in Fig. 1. To test the other cases we have repeated hadron mass measurements for the rest of the boundary conditions on an $8^3 \times (16 \times 2)$ lattice at $m_{sea}a = m_{val}a = 0.01$. The effective masses for π and ρ for the four boundary conditions, plotted in Fig. 4 together with those on a $20^3 \times (20 \times 2)$ lattice, indeed confirm the expectations. The numerical values of meson masses are tabulated in Table III. Similar effects are also observed for the nucleon mass, especially for the (P_{sea}, P_{val}) and (AP_{sea}, P_{val}) boundary conditions (see Table III), while the effect is more complicated for the AP boundary condition for valence quarks due to nonvanishing minimum spatial momentum that contributes to the nucleon mass for this case.

Let us now consider quenched QCD. Since the center

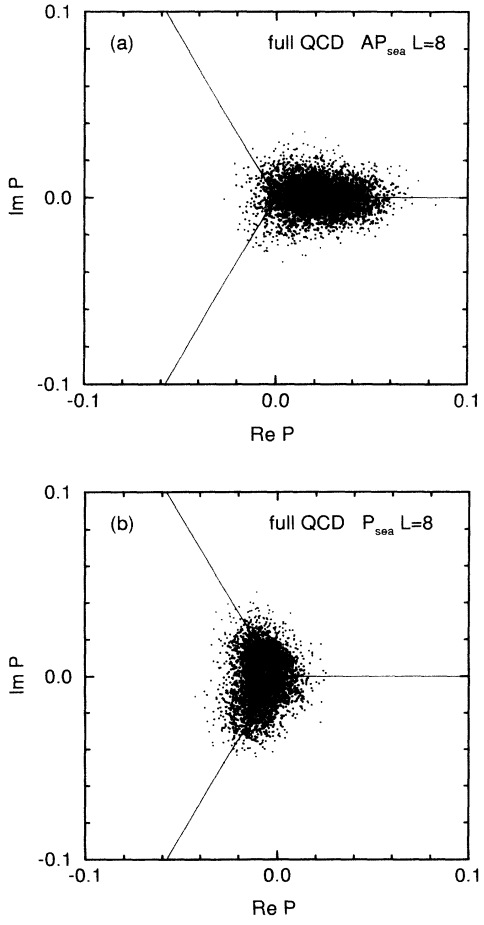

FIG. 3. Distribution of spatial Polyakov loops for full QCD on an $8^3 \times 16$ lattice at $m_q a = 0.01$ with (a) the AP boundary condtion and (b) the P boundary condition for sea quarks.

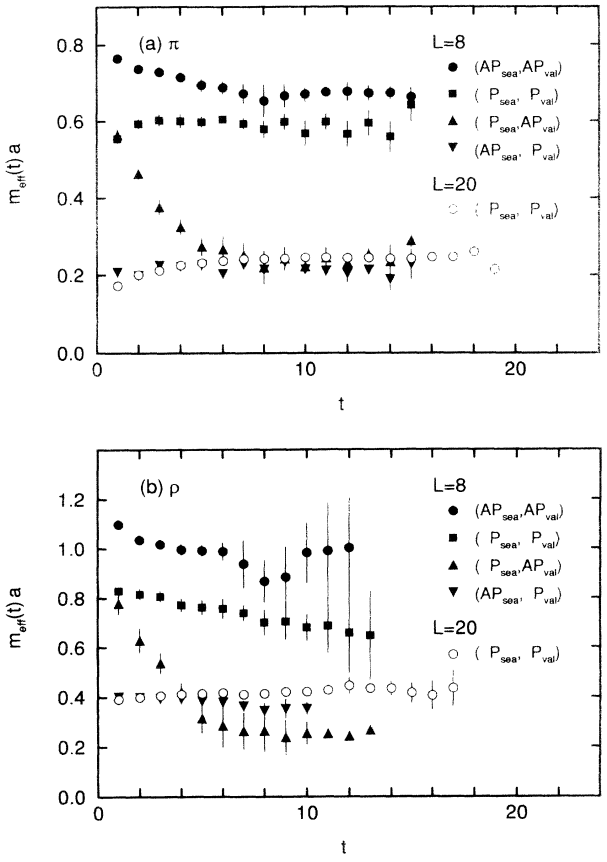

FIG. 4. Effective masses for mesons in full QCD for the four choices of quark boundary conditions on an $8^3 \times (16 \times 2)$ lattice at $m_{sea}a = m_{val}a = 0.01$. (a) π, (b) ρ.

$Z(3)$ is an exact symmetry for a pure gauge action, the distribution of Polyakov loops is symmetric under $Z(3)$ rotations (see Fig. 5 for an example taken on a $6^3 \times 40$ lattice). In this case, average values of Polyakov-type loops vanish unless the winding number of the loop is an integer multiple of 3, whose magnitude would be smaller than those winding only once. This provides a qualitative explanation for smaller finite-size effects observed for quenched hadron masses than those for full QCD.

A small magnitude of Polyakov-type contributions implies that the choice of the boundary condition for the valence quark should have little effect on quenched hadron masses even for small lattice sizes. In Table IV we compare the π, ρ, and N masses for the P and AP bound-

TABLE III. Comparison of full QCD hadron masses on an $8^3 \times (16 \times 2)$ lattice with various boundary conditions for sea and valence quarks. Fitting range is $t \geq 8$ for π and $t \geq 6$ for ρ and N.

b.c. sea	b.c. val.	No. of conf.	$m_\pi a$	$m_\rho a$	$m_N a$
P	P	160	0.581(22)	0.711(42)	1.358(4)
P	AP	160	0.255(16)	0.300(29)	1.367(47)
AP	P	160	0.215(7)	0.357(14)	0.630(22)
AP	AP	160	0.672(17)	0.960(33)	1.584(4)

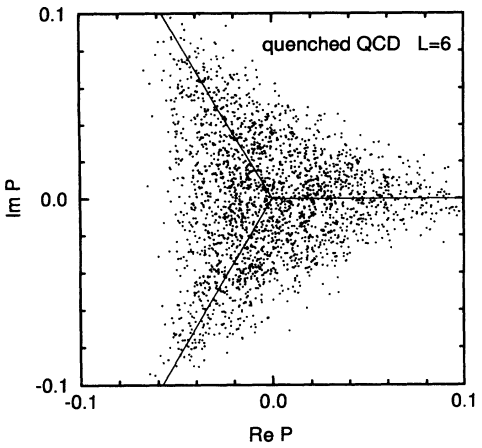

FIG. 5. Distribution of spatial Polyakov loops for quenched QCD on a $6^3\times40$ lattice.

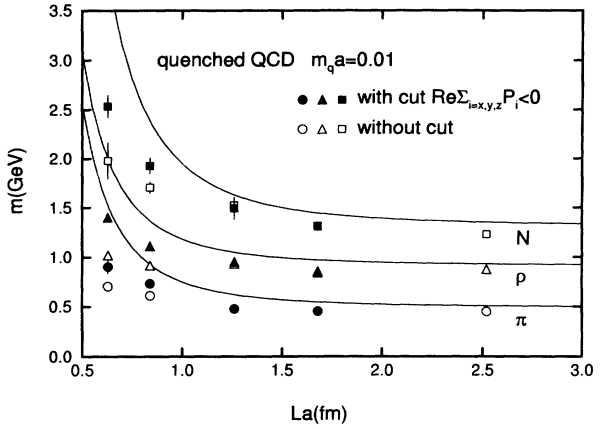

FIG. 6. Comparison of quenched hadron masses at the valence quark mass $m_q a=0.01$ with and without the cut $\mathrm{Re}\sum_{i=x,y,z}P_i<0$ for the spatial Polyakov loop. Filled symbols are with the cut, and open ones without the cut. Solid lines are fits of the form $m=m_\infty+c/L^3$ to full QCD data reproduced from Fig. 1(a).

ary conditions obtained on a $6^3\times40$ lattice. We observe only 10–20% differences for the π and ρ masses between the two boundary conditions (a larger variation for the nucleon mass is due to nonvanishing minimum spatial momentum for the AP boundary condition), whereas in full QCD the masses change by a factor 2–3 on an $8^3\times(16\times2)$ lattice (see Table III) which has a similar physical lattice size $La\approx0.7$ fm.

We should emphasize that the insensitivity of quenched hadron masses to the boundary condition holds only after averaging over a sufficiently large ensemble of gauge configurations having a $Z(3)$-symmetric distribution of Polyakov loops. Configuration by configuration, hadron masses exhibit a finite-size shift whose magnitude and sign vary depending on the spatial Polyakov loops of the configuration in the same way as was discussed above for full QCD; an increase (decrease) for the P boundary condition if the Polyakov loop points in the 1 ($e^{2\pi i/3}$ or $e^{4\pi i/3}$) direction and vice versa for the AP boundary condition. This feature has already been noted in early studies [9,10].

An interesting test related to this point is suggested by a comparison of the distribution of Polyakov loops for quenched and full QCD shown in Figs. 3 and 5. These figures indicate that the configurations for full QCD with the P boundary condition for sea quarks may be mimicked by selecting those pure gauge configurations satisfying $\mathrm{Re}\sum_{i=x,y,z}P_i<0$, where P_i is the Polyakov loop in the ith direction. Quenched hadron masses measured on the selected configurations should increase for the P boundary condition and decrease for the AP boundary condition for the valence quark. The predicted increase for the P boundary condition is verified in Fig. 6, comparing the size dependence of quenched hadron masses with and without the cut $\mathrm{Re}\sum_{i=x,y,z}P_i<0$ (numerical values of hadron masses are listed in Table V). With the cut, the ratio of masses of $L=16$ and 6 lattices increases from $m(L=6)/m(L=16)=1.55$ (π), 1.19 (ρ), and 1.51 (N) to 1.98, 1.66, and 1.94, which are almost as large as the values 2.37, 1.70, and 2.21 for full QCD between a similar range of lattice sizes $L=20$ and 8.

These considerations show that the small finite-size effect for quenched QCD is understood as due to a cancellation among gauge configurations with Polyakov loops falling around the three $Z(3)$ symmetry axes. This also explains the large statistical fluctuations of quenched hadron masses calculated with small-size lattices. In contrast, such a cancellation does not take place in full QCD.

C. Finite-size effect for large volume

Our results and analyses demonstrate that finite-size effects are smaller for quenched QCD. This, however, does not mean that the lattice size of order 2–3 fm currently used in quenched hadron mass measurements is large enough to ignore finite-size errors. Our quenched results are represented in Fig. 7, where π, ρ, and N

TABLE IV. Comparison of quenched hadron masses on a $6^3\times40$ lattice with P and AP boundary conditions for valence quarks. Propagators are fitted over $t\geq6$.

$m_q a$	b.c.	$m_\pi a$	$m_\rho a$	$m_N a$
0.01	P	0.375(11)	0.542(18)	1.053(98)
	AP	0.408(11)	0.641(37)	1.23(41)
0.02	P	0.443(8)	0.588(10)	1.044(66)
	AP	0.463(9)	0.627(20)	1.42(25)

TABLE V. Quenched hadron masses with the cut $\mathrm{Re}\sum_{i=x,y,z}P_i<0$ on an $L^3\times40$ lattice at $m_q a=0.01$, the P boundary condition being used for valence quarks. Propagators are fitted over $t\geq6$.

L	No. of conf.	$m_\pi a$	$m_\rho a$	$m_N a$
6	415	0.480(37)	0.744(20)	1.350(60)
8	300	0.390(10)	0.590(19)	1.025(43)
12	47	0.2547(40)	0.505(20)	0.795(59)
16	31	0.2424(21)	0.448(11)	0.697(23)

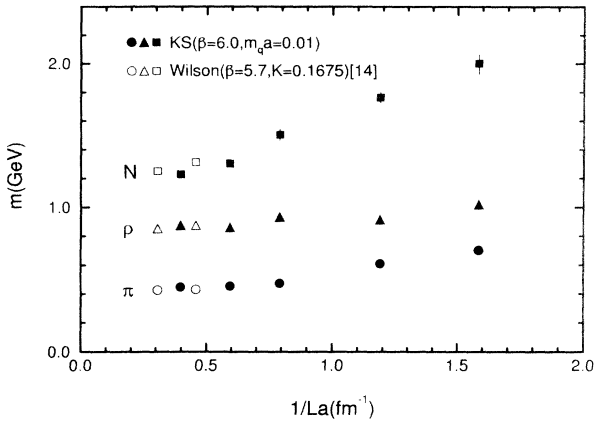

FIG. 7. Quenched hadron masses at $\beta=6.0$ and $m_q a=0.01$ as a function of $1/La$. Open symbols are the GF11 Wilson results at $\beta=5.7$ and $K=0.1675$ with sinks of size 0,1,2 [14].

masses at $m_q a=0.01$ are shown as a function of $1/La$. We also plot the GF11 results [14] for the Wilson action in the quenched approximation obtained with a Gaussian smeared sink of a size 0, 1, and 2 at $\beta=5.7$ and $K=0.1675$, for which $a=0.136$ fm fixed by the ρ meson mass yields hadron mass values similar to those of our Kogut-Susskind results. A particularly conspicuous decrease as a function of the lattice size is seen for the nucleon; we observe a decrease of $(6.5\pm2.3)\%$ between $La\approx1.7$ fm ($L=16$) and the largest lattice size $La\approx2.5$ fm ($L=24$). The nucleon mass at $m_q a=0.02$ also shows a similar decrease, albeit of a smaller magnitude of $(3.5\pm1.4)\%$; this indicates an increasingly important finite-size effect toward the chiral limit. The decrease of the GF11 result extending to a larger lattice size $La\approx3.3$ fm is somewhat less but still significant [$(4.8\pm2.0)\%$ between $La\approx2.2$ fm ($L=16$) and $La\approx3.3$ fm ($L=24$)]. (We should add that no size dependence is found in the GF11 data for the sink size 4 [14] and also in the previous APE Collaboration data for the Wilson action at the same β and lattice sizes [12].)

We expect that the size-dependent shift becomes exponentially small [6] when the size of the lattice is taken sufficiently large compared to the hadron size [5]. A trend of flattening of the size effect for the pion around $1/La\approx(1.25\text{ fm})^{-1}$ may be a symptom for the onset of this behavior. A flattening might also be present in our nucleon mass data between $1/La\approx(1.7\text{ fm})^{-1}$ and $1/La\approx(2.5\text{ fm})^{-1}$. The evidence, however, is too weak to take it as a serious basis for an onset of the exponential behavior toward the infinite-volume limit. An extraction of the value of the nucleon-to-ρ mass ratio in the chiral limit $m_q=0$ is even more problematical; as shown in Fig. 8, the ratio drops by 11% between $La\approx1.7$ fm ($L=16$) and $La\approx2.5$ fm ($L=24$) with no sign observed for the onset of an exponential size dependence. This means that an error possibly as much as 20% may be present in the physical value of m_N/m_ρ predicted in the present simulation.

IV. RESTORATION OF CHIRAL SYMMETRY

In Fig. 9 we show m_π^2 at vanishing quark mass, obtained by an extrapolation of the form

$$(m_\pi a)^2=A_\pi m_q a+B_\pi\ , \tag{3}$$

as a function of the spatial lattice size. A corresponding plot for the value of the chiral condensate linearly extrapolated to $m_q=0$ with the form

$$\langle\bar{\chi}\chi\rangle a^3=A_\chi m_q a+B_\chi \tag{4}$$

is given in Fig. 10. Numerical data for the above are summarized in Table VI.

A marked feature apparent in these figures is a gradual restoration of chiral symmetry for quenched QCD as compared to a rather abrupt restoration at $La\approx1$ fm for full QCD. To understand this difference, let us look once more at Figs. 3 and 5 showing the distribution of spatial

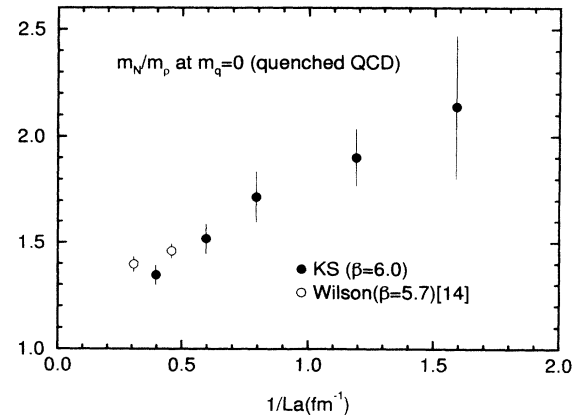

FIG. 8. Quenched m_N/m_ρ as a function of $1/La$ (fm) obtained after extrapolation of hadron masses to the chiral limit $m_q=0$. Open symbols are the GF11 Wilson results at $\beta=5.7$ with sinks of size 0,1,2 [14].

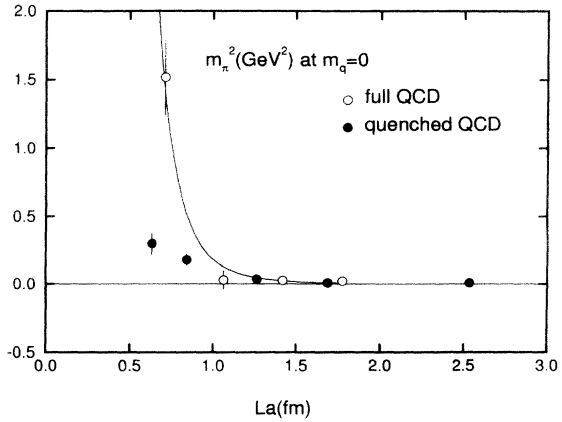

FIG. 9. Size dependence of m_π^2 at $m_q=0$ for full (open symbols) and quenched (filled symbols) QCD. Solid line is a fit of the form $m_\pi=c/L^3$ for full QCD predicted by chiral perturbation theory.

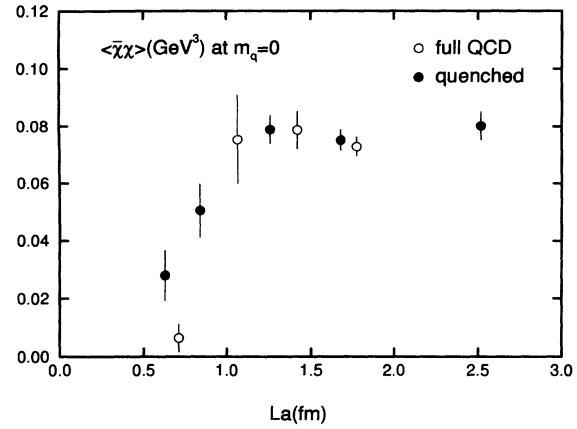

FIG. 10. Size dependence of $\langle\bar{\chi}\chi\rangle$ at $m_q=0$ for full (open symbols) and quenched (filled symbols) QCD.

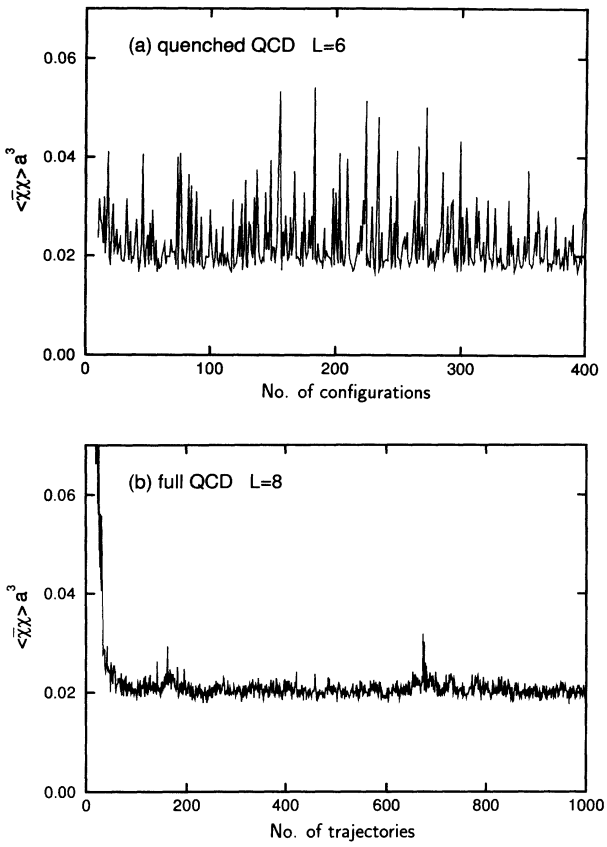

FIG. 11. Comparison of time histories for $\langle\bar{\chi}\chi\rangle$ at $m_q a=0.01$. (a) quenched QCD on a $6^3\times 40$ lattice, (b) full QCD on an $8^3\times 16$ lattice.

Polyakov loops for a small lattice size. For quenched QCD (Fig. 5) the ensemble is a mixture of "confined" configurations with a small value of the Polyakov loop and "deconfined" ones with the Polyakov loop away from the origin toward the $Z(3)$ directions. We expect the former to induce spontaneous breaking of chiral symmetry while the latter tends to restore the symmetry. Thus, signals for restoration of chiral symmetry arising from the deconfined configurations are diluted by the presence of confined ones, leading to a gradual restoration of symmetry. For full QCD, dynamical sea quarks push the bulk of configurations away from the origin (see Fig. 3) at $L=8$. As the size is decreased from $L=12$ ($La\approx 1$ fm) to $L=8$ ($La\approx 0.7$ fm), this causes an abrupt restoration of the symmetry. A support for this picture is provided by the time history of the chiral order parameter shown in Fig. 11. A wild fluctuation observed for the quenched case [Fig. 11(a)] may be interpreted as arising from an alternate occurrence of confined and deconfined configurations. In contrast, the full QCD time history [Fig. 11(b)] exhibits a predominance of small values expected for deconfined configurations.

Let us finally note that chiral perturbation theory predicts that m_π^2 at $m_q=0$ behaves as

TABLE VI. Chiral order parameter and fitted values of $A_{\chi,\pi}$ and $B_{\chi,\pi}$. See Table II for values of $m_\pi a$. Full QCD data are recapitulated from Refs. [1,3] (for $L=16$ values for $A_{\chi,\pi}$ and $B_{\chi,\pi}$ are our estimate using data for $m_q a=0.01$ and 0.02).

			(a) Quenched QCD			
	$\langle\bar{\chi}\chi\rangle a^3$		A_χ	B_χ	A_π	B_π
L	$m_q a=0.01$	$m_q a=0.02$				
6	0.022 77(58)	0.041 38(60)	1.86(83)	0.004 2(13)	5.6(1.1)	0.085(18)
8	0.025 71(56)	0.043 83(85)	1.81(10)	0.007 6(14)	5.48(57)	0.0507(84)
12	0.029 08(35)	0.046 29(28)	1.721(45)	0.011 87(75)	5.68(21)	0.007 1(33)
16	0.028 66(24)	0.046 00(24)	1.734(34)	0.011 32(54)	5.57(12)	0.002 9(18)
24	0.029 39(34)	0.046 70(30)	1.731(45)	0.012 08(74)	5.505(72)	0.001 96(86)
			(b) Full QCD ($N_f=2$)			
	$\langle\bar{\chi}\chi\rangle a^3$		A_χ	B_χ	A_π	B_π
L	$m_q a=0.01$	$m_q a=0.02$				
8	0.020 47(15)	0.040 36(31)	1.989(34)	0.000 58(43)	3.3(3.3)	0.305(55)
12	0.025 76(64)	0.044 74(60)	1.898(88)	0.006 8(14)	8.15(99)	0.006(14)
16[a]	0.027 7(3)	0.048 3(2)	2.060(36)	0.007 1(6)	5.83(21)	0.00 5(3)
20	0.027 55(13)	0.048 52(14)	2.097(19)	0.006 58(30)	5.57(16)	0.00 43(25)

[a]Reference [3].

$$m_\pi \approx \frac{c}{L^3} , \quad (5)$$

with $c = 3/(2f_\pi^2) = 173\ \mathrm{GeV}^{-2}$ for two flavors of dynamical quarks [19]. Fitting the full QCD data in Fig. 10 we obtain a value $c = 90(9)\ \mathrm{GeV}^{-2}$. On the other hand, the increase of the quenched data toward small sizes is too mild to be fitted with this form; the best fit with a power law $m_\pi = cL^{-\alpha}$ yields $\alpha = 1.56(21)$.

V. CONCLUSIONS

In this article we have analyzed the question of whether finite-size effects of hadron masses differ between full and quenched QCD. Our main conclusion is that finite-size effects are much more severe for full QCD. The difference originates from dynamical sea quarks and the associated breaking of the center $Z(3)$ symmetry, which enhance the amplitude for the process of valence quarks propagating around the lattice. In quenched QCD the $Z(3)$ symmetry of the pure gauge action eliminates such amplitudes, and hence leads to smaller finite-size effects. This mechanism is not specific to a particular form of quark action, so that it should apply not only to the Kogut-Susskind quark action, as discussed here, but also to the Wilson quark action as well.

We have found that the finite-size shift of hadron masses is still significant up to a lattice size of $La \approx 2.5-3.3$ fm even in the quenched simulation, especially for the nucleon. Furthermore, the exponential decrease of the size effect expected for large volume is not yet established. We consider that a convincing determination of the nucleon mass (or the nucleon-to-ρ mass ratio) at the few percent level, which is a current goal of quenched QCD, is not possible unless the onset of an exponential size dependence is clearly identified.

ACKNOWLEDGMENTS

Numerical calculations for the present work have been carried out on HITACS 820/80 at KEK. We thank Don Weingarten for data prior to publication and for discussions. This work is supported in part by Grants-in-Aid of the Ministry of Education (Nos. 03640270, 04NP0601, 05640325, and 05640363).

[1] M. Fukugita, H. Mino, M. Okawa, and A. Ukawa, Phys. Rev. Lett. **68**, 761 (1992); M. Fukugita, N. Ishizuka, H. Mino, M. Okawa, and A. Ukawa, Phys. Rev. D **47**, 4739 (1993).

[2] K. M. Bitar *et al.*, Phys. Rev. D **42**, 3794 (1990).

[3] F. R. Brown, F. P. Butler, H. Chen, N. H. Christ, Z. Dong, W. Schaffer, L. I. Unger, and A. Vaccarino, Phys. Rev. Lett. **67**, 1062 (1991); W. Schaffer, in *Lattice '91,* Proceedings of the International Symposium, Tsukuba, Japan, edited by M. Fukugita *et al.* [Nucl. Phys. B (Proc. Suppl.) **26**, 272 (1992)]; in *Lattice '92,* Proceedings of the International Symposium, Amsterdam, The Netherlands, edited by J. Smit and P. van Baal [*ibid.* **30**, 405 (1993)].

[4] C. Bernard, T. Blum, T. A. DeGrand, C. DeTar, S. Gottlieb, A. Krasnitz, R. L. Sugar, and D. Toussaint, Phys. Rev. D **48**, 4419 (1993); in *Lattice '93,* Proceedings of the International Symposium, Dallas, Texas, 1993, edited by T. Draper *et al.* [Nucl. Phys. B (Proc. Suppl.) **34**, (1994)].

[5] M. Fukugita, H. Mino, M. Okawa, G. Parisi, and A. Ukawa, Phys. Lett. B **294**, 380 (1992); in *Lattice '92* [3], p. 365.

[6] M. Lüscher, in *Progress in Gauge Field Theory,* Proceedings of the Cargèse Summer Institute, Cargèse, France, 1983, edited by G. 't Hooft *et al.*, NATO Advanced Study Institutes, Series B: Physics, Vol. 115 (Plenum, New York, 1984); Commun. Math. Phys. **104**, 177 (1986).

[7] D. Toussaint, in *Lattice '91* [3], p. 3.

[8] P. Hasenfratz and I. Montvay, Phys. Rev. Lett. **50**, 309 (1983).

[9] G. Martinelli, G. Parisi, R. Petronzio, and F. Rapuano, Phys. Lett. **122B**, 283 (1983).

[10] R. Gupta and A. Patel, Phys. Lett. **124B**, 94 (1983).

[11] M. Fukugita, T. Kaneko, and A. Ukawa, Nucl. Phys. **B230** [FS10], 62 (1984).

[12] P. Bacilieri *et al.*, Phys. Lett. B **214**, 115 (1988); Nucl. Phys. **B317**, 509 (1989); S. Cabasino *et al.*, in *Lattice '89,* Proceedings of the International Symposium, Capri, Italy, edited by N. Cabibbo *et al.* [Nucl. Phys. B (Proc. Suppl.) **17**, 431 (1990)]; Phys. Lett. B **258**, 195 (1991).

[13] T. Yoshié, Y. Iwasaki, and S. Sakai, in *Lattice '89* [12], p. 413.

[14] F. Butler, H. Chen, J. Sexton, A. Vaccarino, and D. Weingarten, Phys. Rev. Lett. **70**, 2849 (1993); report (unpublished); D. Weingarten (private communication); in *Lattice '93* [4].

[15] P. Bacilieri *et al.*, Nucl. Phys. **B343**, 228 (1990).

[16] R. Gupta, G. Guralnik, G. W. Kilcup, and S. R. Sharpe, Phys. Rev. D **43**, 2003 (1991).

[17] N. Ishizuka, M. Fukugita, H. Mino, M. Okawa, and A. Ukawa, Nucl. Phys. **B411**, 875 (1994).

[18] M. Fukugita, Y. Oyanagi, and A. Ukawa, Phys. Rev. D **36**, 824 (1987).

[19] H. Leutwyler, Phys. Lett. B **189**, 197 (1987).